HHS Public Access

Author manuscript

FEBS J. Author manuscript; available in PMC 2023 June 01.

Published in final edited form as:

FEBS J. 2022 June ; 289(12): 3521–3534. doi:10.1111/febs.16356.

Comparative ligandomics implicates secretogranin III as a disease-restricted angiogenic factor in laser-induced choroidal neovascularization

Liyang Ji[1,2,3],

Prabuddha Waduge[1,2],

Wencui Wan[2,4],

Hong Tian[5],

Jin Li[6],

Jinsong Zhang[3],

Rui Chen[6],

Wei Li[1,2]

[1]Cullen Eye Institute, Department of Ophthalmology, Baylor College of Medicine, Houston, TX, USA.

[2]Bascom Palmer Eye Institute, University of Miami School of Medicine, Miami, FL, USA.

[3]Department of Ophthalmology, The Fourth Affiliated Hospital of China Medical University, Shenyang, Liaoning, China.

[4]Department of Ophthalmology, First Affiliated Hospital of Zhengzhou University, Zhengzhou, Henan, China

[5]Everglades Biopharma, LLC, Houston, TX, USA

[6]Department of Molecular & Human Genetics, Baylor College of Medicine, Houston, TX, USA

Abstract

Choroidal neovascularization (CNV) is a leading cause of vision loss in the elderly. All approved anti-angiogenic drug therapies for CNV target vascular endothelial growth factor (VEGF) but confer limited efficacy. Identification of other CNV-related angiogenic factors will facilitate the development of VEGF-independent alternative therapies. Here, we applied comparative ligandomics to live mice with or without laser-induced CNV for global mapping of CNV-selective endothelial ligands. Secretogranin III (Scg3) previously identified by the same approach as a diabetes-restricted angiogenic factor was mapped with more than 935-fold

Correspondence: Wei Li, Cullen Eye Institute, Baylor College of Medicine, One Baylor Plaza, NC205, Houston, TX, 77030, USA. wei.li4@bcm.edu.

Author Contributions.

LJ, PW and WW designed and performed experiments and data analyses. JL and RC performed NGS analyses. HT provided critical reagents and technical support. JZ provided scientific support. WL supervised and designed the study. LJ and WL wrote the manuscript. All authors approved the final version of the manuscript.

Conflicts of Interest: HT and WL are shareholders of Everglades Biopharma, LLC and LigandomicsRx, LLC. WL is an inventor of issued and pending patents. The remaining authors declare no competing financial interests.

increase in binding to CNV vessels compared to healthy choriocapillaris. A novel *in vivo* ligand binding assay independently confirmed a marked increase in Scg3 binding to CNV vessels, whereas VEGF showed no increase in CNV-selective binding. A new technique of functional immunohistochemistry allowed the visualization and confirmed the increase in *in vivo* Scg3 binding to CNV vasculatures, including CNV microcapillaries with detailed vascular structures, which was blocked by anti-Scg3 humanized antibody Fab fragment (hFab). The hFab effectively alleviated laser-induced CNV with an efficacy similar to the anti-VEGF drug aflibercept. Homozygous deletion of the Scg3 gene in mice significantly reduced the severity of CNV. Furthermore, the therapeutic activity of anti-Scg3 hFab, but not aflibercept, was abolished in $Scg3^{-/-}$ mice, suggesting the Scg3-dependent nature of the hFab-mediated therapy. These findings suggest that Scg3 plays an important role in CNV pathogenesis and is a promising disease-restricted angiogenic factor for ligand-guided disease-targeted anti-angiogenic therapy of CNV.

Graphical Abstract

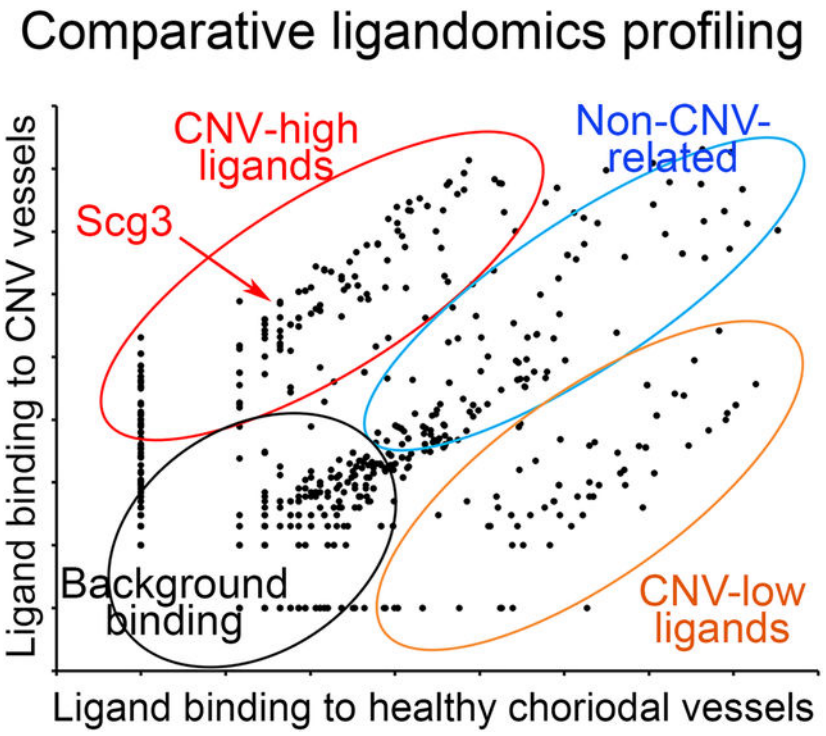

Ligandomics profiling was performed to globally map thousands of endothelial ligands binding to choroidal vessels with or without choroidal neovascularization (CNV) and simultaneously quantify their endothelium-binding activity. Quantitative comparison of entire ligandome profiles for CNV with healthy choroidal vessels systematically mapped CNV-high, CNV-low and non-CNV related endothelial ligands. Secretogranin III (Scg3) was identified as a CNV-high ligand.

Keywords

Secretogranin III; Scg3; choroidal neovascularization; CNV; comparative ligandomics

Introduction

Age-related macular degeneration (AMD), a leading cause of vision loss in people aged 65 and older, is classified into two major categories: wet (exudative or neovascular) and dry (atrophic) AMD [1, 2]. The former with the hallmark of choroidal neovascularization (CNV) accounts for ~10% of total AMD cases but ~90% of all cases with severe vision loss from the disease [3]. Wet AMD is currently treated with anti-angiogenic drugs [4], all of which target vascular endothelial growth factor (VEGF) with limited efficacy [5, 6]. In the absence of other options, patients with poor response to one anti-VEGF drug are often switched to another VEGF blocker, even though these drugs share similar mechanisms of action (MOAs) with limited benefits [7]. Additionally, anti-VEGF may elicit adverse side effects and increase the risk of geographic atrophy [8, 9]. To address these problems, novel therapies against different targets, such as IL-6, RUNX1, aryl hydrocarbon receptor, calreticulin and α2-adrenergic receptor [10–14], have been investigated. Several therapies, including Fovista and nesvacumab targeting respective platelet-derived growth factor and angiopoietin 2, failed in clinical trials of wet AMD [15, 16], probably because of their common VEGF-dependent MOAs [17, 18]. Consequently, an unmet clinical need is to develop novel anti-angiogenic therapies against VEGF-independent pathways for alternative or combination treatment with optimal safety.

We recently identified secretogranin III (Scg3) as a diabetes-selective angiogenic and leakage factor in a mouse model of diabetic retinopathy (DR) by a new technology of comparative ligandomics [19]. The technology is capable of globally mapping cell-binding ligands, simultaneously quantifying their binding activities and systematically comparing their binding activities in diseased versus healthy conditions to delineate disease-selective or restricted ligands. Of thousands of identified retinal endothelial ligands, Scg3 was discovered by comparative ligandomics with the highest binding activity ratio for diabetic versus healthy vessels and the lowest binding to the healthy vasculature [19]. Scg3 was independently verified to drive angiogenesis and promote retinal vascular leakage in diabetic but not healthy mice [19, 20]. In contrast, VEGF binds to and stimulates angiogenesis and leakage of both diabetic and healthy vasculatures. We further generated Scg3-neutralizing monoclonal antibodies (mAbs) that confers high efficacy to alleviate DR leakage in diabetic mice and pathological retinal neovascularization in mouse models of retinopathy of prematurity (ROP) [19, 21]. Subsequently, we confirmed that anti-Scg3 mAb ameliorates CNV in mouse models, including laser-induced CNV (LCNV). Despite these breakthroughs, two questions remain: i) is comparative ligandomics broadly applicable to other vascular diseases beyond DR, such as LCNV? ii) is Scg3 a disease-selective angiogenic factor in LCNV?

Here, we investigated the applicability of comparative ligandomics to LCNV and identified Scg3 as a CNV-selective endothelial ligand. We independently confirmed Scg3 with increased binding to CNV vessels relative to healthy choriocapillaris by a novel *in vivo* ligand binding assay. A new approach of functional immunohistochemistry, which combines *in vivo* ligand binding with conventional immunohistochemistry, visualized Scg3 binding to CNV vessels and microcapillaries that was blocked by a humanized Scg3-neutralizing antibody Fab fragment (hFab). We compared the therapeutic efficacy of the hFab to the

anti-VEGF drug aflibercept for alleviating LCNV. The important role of Scg3 in CNV pathogenesis and its potential as a therapeutic target were independently investigated in $Scg3^{-/-}$ mice.

Results

Profiling of CNV-selective endothelial ligands by comparative ligandomics

To investigate the broad applicability of comparative ligandomics, we applied this approach to mice with or without LCNV lesions for three rounds of *in vivo* binding selection to enrich ligands binding to LCNV vessels or healthy choriocapillaris (Fig. 1A,B). Ligandomics identified a total of 17.30 and 25.19 million valid sequence reads that align to 690 and 800 proteins in the NCBI CCDS database for healthy choriocapillaris and CNV, respectively. Comparative ligandomics identified 226 “LCNV-high” ligands with ≥10-fold increase in binding activity to LCNV vessels vs. healthy choriocapillaris and 121 “LCNV-low” ligands with ≥10-fold decrease in the binding activity. The binding activity plot shows global binding activity changes for all identified ligands, including LCNV-high, LCNV-low, LCNV-unchanged and background binding (Fig. 1C). The Pearson correlation coefficient is calculated as r=0.2174, which is much lower than r=0.489 for DR in 4-month-diabetic mice [19], suggesting dramatic global alternations of endothelial ligand binding profile in acute LCNV vs. chronic DR.

Clonal phage displaying VEGF protein (VEGF-Phage) was spiked into open reading frame phage display (OPD) libraries as an internal control before *in vivo* binding selection and identified by comparative ligandomics with 66 and 90 copies bound to LCNV vessels and healthy choriocapillaris, respectively (Fig. 1D). This binding activity ratio is consistent with 408:2,420 for VEGF-Phage binding to DR:healthy retinal vessels, respectively, in our previous study [19]. In contrast, Scg3 was identified with 65,455 and 70 copies in LCNV and healthy choroids, respectively, implying that Scg3 binding to LCVN vessels dramatically increased by ~935-fold (Fig. 1D), comparable to 1,731:0 for DR:healthy retinal vessels in our previous study [19]. These findings suggest that Scg3, but not VEGF, is a LCNV-selective endothelial ligand.

Independent validation of Scg3 as a LCNV-selective endothelial ligand

Ligands identified by this relatively new technology of ligandomics should be independently verified. Because of the technical challenges for *in vivo* binding assay of endothelial ligands (see Discussion), we recently developed a novel *in vivo* ligand binding assay, which shares similar procedures to ligandomics but used clonal T7 phage displaying Scg3 (Scg3-Phage) or VEGF. After binding and washing by intracardial perfusion, eyes were nucleated, followed by the removal of retinas. We took the advantage of coexistence of healthy choroid and LCNV in the same eye by isolating adjacent but well-separated choroids with versus without CNV in similar tissue sizes. Quantification of vessel-bound phages by plaque assay revealed that Scg3 binding to LCNV increased by 3.13-fold relative to the control choroid and was fully blocked by preincubation with anti-Scg3 hFab (Fig. 2A, C), consistent with the increased Scg3 binding to LCNV profiled by comparative ligandomics (Fig. 1D). Furthermore, preincubation of Scg3-Phage with human rhinovirus

(HRV) 3C protease to cleave and remove Scg3 from the phage surface completely abolished the binding of Scg3-Phage to LCNV vessels (Fig. 2A, C). These results suggest that the increased binding of Scg3-Phage was not due to increased permeability of CNV vessels and phage leakage from the vasculature.

However, we failed to detect a significant increase of VEGF-Phage binding to LCNV over healthy choriocapillaris (Fig. 2B), consistent with the minimal increase in VEGF binding to LCNV detected by comparative ligandomics (Fig. 1D). VEGF-Phage binding to healthy and CNV vessels was not blocked by aflibercept, suggesting minimal VEGF-specific binding in both conditions. Furthermore, pretreatment with HRV 3C protease failed to further reduce already minimal VEGF binding to healthy or LCNV vessels. These data confirm that VEGF minimally binds to healthy and LCNV vessels and that Scg3, but not VEGF, represents a CNV-selective angiogenic factor.

Visualize Scg3 binding to LCNV *in vivo* by functional immunohistochemistry

To further confirm Scg3 binding to LCNV vessels, we developed a new technique of functional immunohistochemistry to visualize Scg3 binding to vasculatures by combining *in vivo* ligand binding with conventional immunohistochemistry. To improve detection sensitivity, we labeled each Scg3-Phage particle with ~400 copies of FLAG tag by amplifying Scg3-Phage in BLT7FLAG bacteria [22], performed *in vivo* binding with purified FLAG-tagged Scg3-Phage. After sequential intracardial perfusion with PBS to remove unbound phages and 4% paraformaldehyde to fix vessel-bound Scg3-Phage in situ and prevent ligand-receptor dissociation, vessel-bound FLAG-tagged Scg3-Phage was visualized by immunohistochemistry using anti-FLAG mAb. The results show that Scg3-Phage bound to LCNV and was blocked by preincubation with anti-Scg3 hFab (Fig. 2D, Column 2 vs. 4), consistent with its binding quantification in Fig. 2A. The zoom-in image reveals that FLAG-tagged Scg3-Phage bound to LCNV vessels with detailed structure of microcapillaries (Fig. 2D, Column 3, top panel). No Scg3-Phage leakage from the fenestrated choroidal vessels was detected. As a control, Scg3-Phage failed to bind to healthy choroids (Fig. 2D, Column 1). In contrast, FLAG-tagged VEGF-Phage showed equal background binding in the absence and presence of aflibercept (Fig. 2D, Column 4 vs. 5).

Minimal increase in Scg3 expression in LCNV

An interesting question is whether Scg3 expression increases in LCNV. We analyzed Scg3 expression in LCNV and healthy choroids by conventional immunohistochemistry using anti-Scg3 antibody and detected similar Scg3 levels in both conditions (Fig. 2E). These findings are consistent with our previous studies that Scg3 is not induced in DR despite its increased binding to DR vessels [19].

In vitro neutralizing activity of anti-Scg3 hFab

To facilitate the translation of anti-Scg3 therapy, we converted one of the optimal Scg3-neutralizing mAbs to a humanized anti-Scg3 hFab. Here we further confirmed the Scg3-neutralizing activity of the hFab using two *in vitro* functional assays. In the first assay, Scg3-induced wound healing migration of human umbilical vein endothelial cells (HUVECs) was

blocked by anti-Scg3 hFab (Fig. 3A,B). As a positive control, VEGF-induced migration of HUVECs was also inhibited by aflibercept. In the second assay, Scg3 significantly stimulated tube formation of HUVECs with increased tube number, tube length and branch points, and anti-Scg3 hFab blocked Scg3-induced tube formation (Fig. 3C–F). Likewise, VEGF as a positive control promoted tube formation of HUVECs that was blocked by aflibercept. These studies confirmed the neutralizing activity of anti-Scg3 hFab.

In vivo therapeutic efficacy of anti-Scg3 hFab

To investigate the therapeutic potential of anti-Scg3 hFab, we compared its efficacy to aflibercept for alleviating LCNV in mice via intravitreal administration. H&E staining of retinal sections showed both anti-Scg3 hFab and aflibercept intravitreally injected 3 days (D3) post laser photocoagulation reduced LCNV lesion size in mice at D7 (Fig. 4A). To quantitatively assess the therapeutic efficacy, we analyzed CNV leakage at D7 using fluorescein angiography (FA) and confirmed that intravitreal anti-Scg3 hAb at 2 μg/eye significantly inhibited CNV leakage, including leakage intensity and area, with similar efficacy to aflibercept (Fig. 4B–D). We further isolated eyecups of the retinal pigment epithelium (RPE)-choroid-sclera complex (RPE eyecups) on D7, stained CNV vessels with Alexa Fluor 488 (AF488)-isolectin B4 (IB4) and analyzed the CNV vasculature. The results indicated that anti-Scg3 hFab and aflibercept conferred similar efficacy to significantly reduce CNV maximal area and 3D volume (Fig. 4E–G). In these studies, control hFab was included as a negative control. These findings suggest that anti-Scg3 hFab is a potent anti-angiogenic agent for LCNV therapy.

Deletion of Scg3 alleviates LCNV severity and nullifies anti-Scg3 hFab efficacy

$Scg3^{-/-}$ mice were reported with normal gross phenotypes, including body weight, behavior and fertility [23]. Given that Scg3 shares minimal amino acid sequence homology to other proteins, Scg3-knockout (KO) mice provide a convenient model to assess the pathological role of Scg3 in CNV pathogenesis. We quantified and compared the severity of LCNV in wild-type and Scg3-null mice and found that the latter had markedly reduced CNV leakage area size and intensity, as analyzed by FA (Fig. 5A–C). CNV vessel staining also indicated that $Scg3^{-/-}$ mice had reduced CNV 3D volume and lesion size. (Fig. 5D–F).

To determine whether anti-Scg3 hFab may alleviate CNV through off-target effects, we analyzed its therapeutic activity in $Scg3^{-/-}$ mice. The results showed that aflibercept efficiently inhibited LCNV in both wild-type and Scg3-deficient mice, including CNV leakage size and area by FA imaging and CNV 3D volume and lesion size by the vessel staining (Fig. 6). In contrast, anti-Scg3 hFab ameliorated LCNV only in wild-type but not Scg3-null mice (Fig. 6). In these studies, naïve hFab was included as a negative control. These results suggest that Scg3 plays an important role in the pathogenesis of LCNV and that anti-Scg3 hFab alleviates CNV through a Scg3-dependent manner.

Discussion

Despite advancements in functional proteomics to profile intracellular protein-protein interactomes [24], ligand-receptor interactions (LRIs) on the cell surface remain to be

identified on a case-by-case basis. Single-cell RNA-seq has been used to infer only known LRIs but is incapable of deducing unknown LRIs [25]. To address the challenge, we recently developed ligandomics technology capable of identifying known as well as unknown LRIs based on experimental protein-protein interactions [19, 26]. In a previous study, we applied comparative ligandomics to diabetic vs. healthy mice, globally mapped DR-related endothelial ligands and discovered Scg3 as a novel DR-selective ligand that preferentially binds to DR vs. healthy retinal vessels [19]. In contrast, VEGF binds to both DR and healthy vasculatures equally well. Independent validation confirmed that Scg3 preferentially induces angiogenesis and vascular leakage in diabetic over healthy mice, whereas VEGF promotes angiogenesis and permeability of both diabetic and healthy vessels [20]. These findings established the validity of comparative ligandomics.

An important question is whether ligandomics is broadly applicable to other vascular diseases. This study applied comparative ligandomics to LCNV and healthy choroids, globally mapped CNV-high and low ligands and identified Scg3 as a CNV-high endothelial ligand. Based on LRIs and pharmacological MOAs, we predict that CNV-high ligands are more promising therapeutic targets than CNV-low ligands, because therapies targeting CNV-low ligands with reduced receptor expression on CNV vessels will exert diminished modulatory effects on diseased vessels. In the extreme case with completely abolished receptor expression, no therapies targeting the cognate ligands can exert any effects on diseased vasculatures. In addition to Scg3, other identified CNV-high endothelial ligands are currently under independent characterization for their binding selectivity, functional activity, pathogenic role and therapeutic potential. Some validated CNV-high ligands are under investigation for drug development. These results suggest that ligandomics is broadly applicable to vascular diseases beyond DR and is a valuable tool for drug target discovery.

We recently proposed that an angiogenic factor can contribute to pathological neovascularization through upregulation of the angiogenic ligand itself, its cognate receptor or both [26]. Our previous study showed that anti-Scg3 mAb alleviates CNV high efficacy [27], implying that Scg3 may contribute to CNV pathogenesis through one of these modes. We previously reported that Scg3 is minimally upregulated in mouse models of DR and ROP [19]. Similarly, immunohistochemistry in this study confirmed that Scg3 expression is not upregulated in LCNV (Fig. 2E), implicating that Scg3 binding upregulation may confer CNV pathogenesis. Indeed, comparative ligandomics found that Scg3 is a CNV-high endothelial ligand. This result is supported by independent *in vivo* ligand binding assay and functional immunohistochemistry using clonal Scg3-Phage (Fig. 2A–D).

An interesting question is the huge discrepancy in Scg3 binding activity quantification by comparative ligandomics versus clonal Scg3-Phage ligand binding assay. The former detected ~935-fold increase in Scg3 binding to LCNV relative to healthy choriocapillaris (Fig. 1D), whereas the latter found only 3.13-fold (Fig. 2A). This discrepancy is likely due to differences in technical platforms between these two assays. Ligandomics detected and quantified cDNA copy number of vessel-bound Scg3-displaying library phages by next-generation DNA sequencing (NGS) after PCR amplification, whereas ligand binding assay detected vessel-bound clonal Scg3-Phage by plaque assay. The presence of trillions of other OPD library clones in ligandomics profiling competitively reduced non-specific

binding of library Scg3 clones with only 70 copies of Scg3 cDNA inserts detected for healthy vessels (Fig. 1D). In contrast, the ligand binding assay with clonal Scg3-Phage lacked the competitive blockade of non-specific binding by library clones and had much higher background binding with 11,515 plaque forming unit (pfu)/mg tissue detected in healthy choroids (Fig. 2A). The high background binding may derive from non-specific phage binding to choroidal endothelia through Scg3 displayed on phage surface as well as other phage own surface proteins (e.g., capsid and tail fiber proteins). As a result, the Scg3-Phage binding increase to CNV vessels was markedly reduced to only 3.13-fold in the binding assay, which more closely resembles traditional binding assays with protein ligands than ligandomics. These data suggest that Scg3 receptor(s) (Scg3R) expression is markedly upregulated in CNV vessels. The identity of the Scg3R is currently under intense investigation (unpublished data).

Another question is why minimal VEGF binding was detected (Fig. 1D, 2B, 2D), even though VEGF regulation of CNV vessels was therapeutically detected by aflibercept (Fig. 4). Both Scg3-Phage and VEGF-Phage have been validated *in vitro* for their binding to anti-Scg3 hFab and aflibercept and competitively blocked by recombinant protein Scg3 and VEGF, respectively [28]. These results suggest that Scg3 and VEGF displayed on phage surface have conformations closely related to their native proteins. Furthermore, the binding of VEGF-Phage to human retinal microvascular endothelial cells and SK-N-AS neuroblastoma cell line was significantly blocked by aflibercept [28]. Thus, minimal detection of aflibercept-sensitive VEGF-Phage binding in Fig. 2B and 2D suggests the low expression of VEGF receptors (VEGFRs) on both healthy choriocapillaris and LCNV vessels in adult mice. Likewise, minimal VEGF-Phage binding to mature retinal vasculature in adult mice with or without DR was detected (unpublished data). In contrast, *in vivo* ligand binding and functional immunohistochemistry detected aflibercept-sensitive VEGF-Phage binding to the developing retinal vasculature of neonatal mice at postnatal day 17 with or with oxygen-induced retinopathy [28]. These findings suggest that VEGFRs are mostly expressed on neonatal retinal vessels but minimally on mature retinal and choroidal vasculatures. This may also explain why preterm ROP infants are more susceptible to adverse side effects of anti-VEGF therapy than adults or the elderly with DR or wet AMD [29].

In vivo ligand binding and functional immunohistochemistry are new techniques developed by our group. VEGF *in vivo* binding has hitherto been impossible because VEGF dimer with only 45 kDa can readily leak out of vasculatures and be trapped in the extravascular space [30, 31]. Furthermore, choriocapillaris is well-characterized fenestrated vessels that are permeable to proteins less than ~232 kDa or 5.5 nm in diameter [32, 33]. We previously discussed that ligands displayed on the surface of the T7 phage with ~55 nm in diameter, equivalent to ~90,000 kDa, are impermeable to both healthy and diseased vessels [19]. Indeed, the zoom-in image of FLAG-tagged Scg3-Phage binding to CNV microcapillaries without any sign of signal diffusion is indicative of no phage leakage (Fig. 2D, Column 3, top panel).

Scg3 belongs to the granin family that comprises chromogranin A (CgA), CgB, secretogranin II (Scg2, or SgII), HISL-19 antigen (SgIV), neuroendocrine secretory protein

7B2 (SgV), NESP55 (SgVI), nerve growth factor inducible protein VGF (SgVII), and proSAAS (SgVIII) [34]. The family plays an important role in the biogenesis of secretory granules, including protein sorting, proteolytic cleavage of prohormones, secretory vesicle formation and condensation. In contrast to other protein families defined by sequence homology, such as VEGF protein family [35], the granin family is formed by arbitrary criteria of their biochemical and structural characteristics. These include their localization in secretory vesicles, acidic isoelectric point (pI), calcium-binding activity, propensity to form aggregates and presence of multiple dibasic cleavage sites [34]. Although Scg3 shares no significant sequence homology to any other proteins, including granins, $Scg3^{-/-}$ mice apparently develop normal gross phenotypes, including body weight, behavior and fertility, without defect in the secretion of vital hormones, such as insulin [23]. Our studies confirmed normal ocular phenotype of Scg3-null mice (Fig. 5, 6) [28]. Detailed analyses revealed only subtle metabolic defects in $Scg3^{-/-}$ mice, including maladaptation of endocrine cells to inadequate diet and stress by impairing the proteolytic conversion of prohormones in secretory granules [36]. Single-nucleotide polymorphisms in the Scg3 gene influence the risk of obesity by regulating the secretion of hypothalamic appetite-related neuropeptides [37]. The results suggest that intracellular role of Scg3 to regulate the biogenesis of secretory granules can be largely compensated by other granins, despite the lack of sequence homology.

CgA and Scg2 were reported to regulate angiogenesis with bifunctional activities. While Scg2-derived secretoneurin is proangiogenic [38, 39], Scg2 was recently reported to directly promote HIF-1α degradation, downregulate VEGF expression and inhibit tumor growth and angiogenesis [40]. Similar bifunctional activities were also reported for CgA that can be proteolytically processed into pro- or anti-angiogenic polypeptides [34, 41, 42]. Interestingly, Scg3 upregulation was reported in several tumors, including neuroendocrine tumors, small cell lung cancer and glioma [43–45]. However, it is controversial whether Scg3 is a positive or negative prognostic factor for tumors [43, 45]. Because of their minimal sequence homology, Scg3 may not share similar molecular mechanisms with CgA and Scg2 to regulate angiogenesis. Anti-Scg3 hFab with no access to intracellular compartments should not interfere with its functional role in regulating biogenesis of secretory granules.

All currently approved drug therapies for neovascular AMD target VEGF, and about half of the patients after the treatment have limited efficacy to improve vision with potential adverse side effects on healthy vessels and cells [5, 6, 8, 21, 46]. VEGF is a well-known growth and survival factor for endothelial cells as well as neurons and RPE cells [47, 48]. Excessive anti-VEGF treatment may result in significant CNV regression but minimal improvement in vision. For example, clinical studies reported that ranibizumab in excessively high doses had worse improvements in visual acuity than in moderate doses, despite marked improvements in the anatomical structure of the retina [49, 50]. Moreover, anti-VEGF therapy may increase the risk of geographic atrophy with the degeneration of RPE and photoreceptors [8, 9]. Therefore, developing novel disease-targeted anti-angiogenic therapies against VEGF-independent targets will help improve treatment efficacy and circumvent adverse side effects. Indeed, our recent studies detected significant safety advantages of anti-Scg3 mAb and hFab over aflibercept in animal models [21, 28].

In summary, this study identified Scg3 as a CNV-restricted endothelial ligand by comparative ligandomics and independently confirmed the finding by *in vivo* ligand binding assay and functional immunohistochemistry. *In vivo* studies in wild-type and Scg3-KO mice confirmed that Scg3 is a therapeutic target for CNV and that anti-Scg3 hFab alleviates CNV with high efficacy. Because of its disease selectivity with minimal binding to no CNV vessels, anti-hFab has the potential to be developed as the next-generation disease-targeted anti-angiogenic therapy for ocular vascular diseases with optimal safety.

Materials and Methods

Animals and materials

C57BL/6J mice (6–8 weeks old) were purchased from the Jackson Laboratory (Bar Harbor, ME). Scg3-KO mice were from Taconic Biosciences (Model #TF3191) and were backcrossed to C57BL/6J mice for at least five generations. $Scg3^{-/-}$ mice were verified by genotyping (not shown), reverse transcription-PCR and Western blot (unpublished data). All animal procedures were approved by the Institutional Animal Care and Use Committee at the University of Miami or Baylor College of Medicine.

Anti-Scg3 hFab was engineered from a mouse mAb by Everglades Biopharma, LLC and was characterized in a separate study [28]. HUVECs previously described [51] were used in this study because commercial human choroidal endothelial cells failed to develop VEGF-induced tube formation and express minimal CD31 (data not shown). VEGF-Phage displaying VEGF110 was described in a recent study [19]. Scg3-Phage displaying full-length human Scg3 was constructed in a similar manner [19].

LCNV

CNV was generated as previously described [52]. Briefly, C57BL/6J and Scg3 KO mice were subjected to laser photocoagulation (Argon laser, 532 nm, 100 mW, 0.8 s, 50 μm, 4 spots per retina around the optic disc) on Day 0 (D0) using MICRON IV system (Phoenix). Lesions with choroidal hemorrhage on D0 and linear or fused lesions on D7 were excluded.

Comparative ligandomics

Ligandomics was carried out, as described [19]. Briefly, OPD libraries from mouse adult eyes and E18 embryos were amplified in BLT5615 bacteria and combined. VEGF-Phage was amplified and diluted into the combined libraries (1:1,000), which were purified by CsCl gradient centrifugation, dialyzed against PBS and titrated by plaque assay. Purified library phages were injected i.v. (1×10^{12} pfu/mouse, 200 μl/mouse) into LCNV mice at D7 post laser photocoagulation and healthy mice (six eyes per group for Round 1 and four eyes for Round 2 and 3). After circulation for 20 min, mice were euthanized by CO_2 inhalation, immediately followed by intracardial perfusion with PBS (10 ml/min) to remove unbound phages. After the removal of retinas from enucleated eyes, CNV lesions were precisely dissected along the demarcation line of the lesion from RPE eyecups under a dissecting microscope. Control RPE eyecups in approximately equivalent area size were isolated from healthy mice. Isolated tissues were weighed and homogenized in PBS with 1% Triton X-100 to release vessel-bound phages. After titration by plaque assay, released phages were

amplified in BLT5615 bacteria, purified as above, and used as input for the next round of *in vivo* binding selection in mice with or without LCNV (Fig. 1A). A total of three rounds of the binding selection were performed to enrich endothelium-binding phages. cDNA library inserts of enriched phages were amplified by PCR, purified on agarose gels and analyzed by NGS. Identified sequences were aligned against the NCBI CCDS database [19].

In vivo ligand binding assay

Clonal Scg3-Phage and VEGF-Phage were amplified in BLT5615 bacteria, purified, titrated, preincubated with or without anti-Scg3 hFab (4 μg/ml) or aflibercept (4 μg/ml), respectively, and injected i.v. into mice with LCNV on D7 post laser photocoagulation (1×10^{12} pfu/mouse). After circulating for 20 min, mice were euthanized by CO_2 inhalation and immediately subjected to intracardial perfusion with 70 ml PBS for 7 min to wash out unbound phages. Choroids with or without CNV lesion in similar sizes were isolated from the same RPE eyecups, weighed and homogenized in PBS with 1% Triton X-100 to release vessel-bound phages, which were quantified by plaque assay. To determine ligand-binding specificity and background binding, we also preincubated Scg3-Phage and VEGF-Phage with HRV 3C protease (100 units/ml, ACROBiosystems, Cat. # 3CC-N3133) at 4°C overnight to release Scg3 or VEGF from the phage surface before the binding assay [22].

Immunohistochemistry

Mice with or without LCNV were euthanized with CO_2 inhalation 7 days post laser photocoagulation and perfused with PBS and 4% paraformaldehyde. Enucleated eyes were re-fixed and embedded in optimal cutting temperature compound (OCT). Cryosections of eyes in 6-μm thickness were immunostained with anti-Scg3 rabbit polyclonal antibody (Proteintech, #10954-AP, 1:50) [19] and anti-CD31 mouse mAb (Abcam, #ab24590, 1:250), followed by Alexa Fluor 594 (AF594)-conjugated anti-rabbit IgG F(ab')2 (Cell Signaling, #8889S; 1:1000) and AF488-conjugated anti-mouse Ab (Abcam, #ab150113; 1:500) and analyzed using a Keyence BZ-X810 structured illumination microscope (SIM).

Functional immunohistochemistry

Scg3-Phage and VEGF-Phage were amplified in BLT7FLAG bacteria to label phage capsid 10A protein with FLAG tag, as described [22]. Amplified phages were purified and injected i.v. into anesthetized mice with or without LCNV for *in vivo* ligand binding as described above. After intracardial perfusion with PBS, mice were further perfused with 4% paraformaldehyde to fix vessel-bound phages *in situ* to prevent ligand-receptor dissociation. Eyes were enucleated, embedded in OCT, cryosectioned and immunostained with anti-FLAG mAb (Sigma, #F1804, 1:200), followed by AF594 anti-mouse Ab (Abcam, #ab150113; 1:500) and AF488-IB4 (10 μg/ml) and analyses using the SIM.

In vitro migration assay

Endothelial wound healing migration assay was conducted as described [51]. Briefly, HUVECs were seeded overnight at 90% confluency in 12-well plates precoated with 1% gelatin. A scratch with approximately 1 mm in width in each well was created using sterile

200-μl pipette tips. After the removal of dislodged cells by washing, Scg3 (1 μg/ml), VEGF (100 ng/ml) or PBS was added to HUVECs in the presence or absence of anti-Scg3 hFab (5 μg/ml) or aflibercept (1.5 μg/ml), respectively. Migration of cells was monitored at 0 and 24 h under a light microscope. The denuded area covered by migrated cells was quantified using ImageJ software (NIH).

Endothelial tube formation assay

The assay was performed as previously described [51]. In brief, after starvation for 3 h in serum-free EBM-2 medium (Lonza), HUVECs were seeded on 96-well plates precoated with growth factor-reduced Matrigel (Corning Life Science, Cat. #354263) in EBM-2 medium. Scg3 (300 μg/ml), VEGF (50 ng/ml) or PBS was added to HUVECs with or without anti-Scg3 hFab (1.5 μg/ml) or aflibercept (500 ng/ml), respectively. After incubation for 4 h, cells were photographed under a light microscope and quantified for tube number, tube length and branch points per viewing field using ImageJ.

Therapy of LCNV

Anti-Scg3 hFab, aflibercept, or control human IgG Fab (2 μg/1μl/eye) was blind coded and intravitreally injected on D3 post laser photocoagulation. FA was conducted on D7. All FA images were taken 6 min post injection of fluorescein sodium (0.1 ml, 2.5 %) in anesthetized mice with standardized instrument settings. FA images were analyzed by ImageJ. The intensity of the laser spots was normalized to cognate entire viewing field of the eye. After FA, RPE eyecups were harvested from euthanized mice, fixed, stained with AF488-IB4 (10 μg/ml) [27], flat-mounted, imaged using the SIM and analyzed using the Keyence software.

H & E staining

Eyeballs were collected on D7 post laser photocoagulation. After fixation in Davidson's solution [53] overnight, they were embedded in OCT, cryosectioned and stained with H&E.

Statistics

NGS data analyses were performed, as described [19]. Other data are shown as mean ± SEM and analyzed by one-way ANOVA or Student's t-test.

Acknowledgments.

We thank Dr. Yingbin Fu for scientific discussion and instruments. This work was partially supported by NIH R01EY027749 (W.L.), R24EY028764 (W.L. and K.A.W.), R24EY028764-01A1S1 (W.L. and K.A.W.), R43EY031238 (H.T., K.A.W. and W.L.), R43EY031643 (H.T.), R43EY032827 (H.T. and W.L.), R41EY027665 (W.L. and H.T.), American Diabetes Association 1-18-IBS-172 (W.L.), NIH P30EY002520, P30EY014801, Knights Templar Eye Foundation Endowment in Ophthalmology (W.L.) and unrestricted institutional grants from Research to Prevent Blindness (RPB) to Department of Ophthalmology, University of Miami and Department of Ophthalmology, Baylor College of Medicine. NGS was performed on an Illumina sequencer supported by NIH shared instrument grant S10OD023469 (R.C).

Abbreviations

AF488	Alexa Fluor 488

AF594	Alexa Fluor 594
AMD	age-related macular degeneration
CgA	chromogranin A
CNV	choroidal neovascularization
DR	diabetic retinopathy
FA	fluorescein angiography
hFab	humanized antibody Fab fragment
HRV	human rhinovirus
HUVEC	human umbilical vein endothelial cell
IB4	isolectin B4
KO	knockout
LCNV	laser-induced CNV
LRI	ligand-receptor interaction
mAb	monoclonal antibody
MOA	mechanisms of action
NGS	next-generation DNA sequencing
OCT	optimal cutting temperature compound
OPD	open reading frame phage display
ROP	retinopathy of prematurity
RPE	retinal pigment epithelium
Scg2	secretogranin II
Scg3	secretogranin III
Scg3R	Scg3 receptor
SIM	structured illumination microscope
VEGF	vascular endothelial growth factor
VEGFR	VEGF receptor

References

1. Wong WL, Su X, Li X, Cheung CMG, Klein R, Cheng C-Y, Wong TY (2014) Global prevalence of age-related macular degeneration and disease burden projection for 2020 and 2040: a systematic review and meta-analysis. Lancet Glob Health 2, e106–116. [PubMed: 25104651]

2. Ambati J, Fowler BJ (2012) Mechanisms of age-related macular degeneration. Neuron 75, 26–39. [PubMed: 22794258]

3. Votruba M, Gregor Z (2001) Neovascular age-related macular degeneration: present and future treatment options. Eye (Lond) 15, 424–429. [PubMed: 11450768]

4. Papadopoulos Z (2020) Recent Developments in the Treatment of Wet Age-related Macular Degeneration. Curr Med Sci 40, 851–857. [PubMed: 32980899]

5. Brown DM, Michels M, Kaiser PK, Heier JS, Sy JP, Ianchulev T, ANCHOR Study Group (2009) Ranibizumab versus verteporfin photodynamic therapy for neovascular age-related macular degeneration: Two-year results of the ANCHOR study. Ophthalmology 116, 57–65.e5. [PubMed: 19118696]

6. Rosenfeld PJ, Brown DM, Heier JS, Boyer DS, Kaiser PK, Chung CY, Kim RY, MARINA Study Group (2006) Ranibizumab for neovascular age-related macular degeneration. N Engl J Med 355, 1419–1431. [PubMed: 17021318]

7. Pinheiro-Costa J, Costa JM, Beato JN, Freitas-da-Costa P, Brandao E, Falcao MS, Falcao-Reis F, Carneiro AM (2015) Switch to Aflibercept in the Treatment of Neovascular AMD: One-Year Results in Clinical Practice. Ophthalmologica 233, 155–161. [PubMed: 25896317]

8. Grunwald JE, Pistilli M, Daniel E, Ying G-S, Pan W, Jaffe GJ, Toth CA, Hagstrom SA, Maguire MG, Martin DF, et al. (2017) Incidence and Growth of Geographic Atrophy during 5 Years of Comparison of Age-Related Macular Degeneration Treatments Trials. Ophthalmology 124, 97–104. [PubMed: 28079023]

9. Grunwald JE, Pistilli M, Ying G-S, Maguire MG, Daniel E, Martin DF, Comparison of Age-related Macular Degeneration Treatment Trials Research Group (2015) Growth of geographic atrophy in the comparison of age-related macular degeneration treatments trials. Ophthalmology 122, 809–816. [PubMed: 25542520]

10. Choudhary M, Safe S, Malek G (2018) Suppression of aberrant choroidal neovascularization through activation of the aryl hydrocarbon receptor. Biochim Biophys Acta Mol Basis Dis 1864, 1583–1595. [PubMed: 29481912]

11. Tanaka M, Inoue Y, Imai T, Tanida N, Takahashi K, Hara H (2021) Guanabenz and Clonidine, α2-Adrenergic Receptor Agonists, Inhibit Choroidal Neovascularization. Curr Neurovasc Res 18, 85–92. [PubMed: 34011258]

12. Bee Y-S, Ma Y-L, Chen J, Tsai P-J, Sheu S-J, Lin H-C, Huang H, Liu G-S, Tai M-H (2018) Inhibition of Experimental Choroidal Neovascularization by a Novel Peptide Derived from Calreticulin Anti-Angiogenic Domain. Int J Mol Sci 19, E2993. [PubMed: 30274378]

13. Gonzalez-Buendia L, Delgado-Tirado S, An M, O'Hare M, Amarnani D, Whitmore HAB, Zhao G, Ruiz-Moreno JM, Arboleda-Velasquez JF, Kim LA (2021) Treatment of Experimental Choroidal Neovascularization via RUNX1 Inhibition. Am J Pathol 191, 418–424. [PubMed: 33345998]

14. Droho S, Cuda CM, Perlman H, Lavine JA (2021) Macrophage-derived interleukin-6 is necessary and sufficient for choroidal angiogenesis. Sci Rep 11, 18084. [PubMed: 34508129]

15. Apte RS, Chen DS, Ferrara N (2019) VEGF in Signaling and Disease: Beyond Discovery and Development. Cell 176, 1248–1264. [PubMed: 30849371]

16. Dunn EN, Hariprasad SM, Sheth VS (2017) An Overview of the Fovista and Rinucumab Trials and the Fate of Anti-PDGF Medications. Ophthalmic Surg Lasers Imaging Retina 48, 100–104. [PubMed: 28195611]

17. Wang D, Huang HJ, Kazlauskas A, Cavenee WK (1999) Induction of vascular endothelial growth factor expression in endothelial cells by platelet-derived growth factor through the activation of phosphatidylinositol 3-kinase. Cancer Res 59, 1464–1472 [PubMed: 10197615]

18. Lobov IB, Brooks PC, Lang RA (2002) Angiopoietin-2 displays VEGF-dependent modulation of capillary structure and endothelial cell survival in vivo. Proc Natl Acad Sci U S A 99, 11205–11210. [PubMed: 12163646]

19. LeBlanc ME, Wang W, Chen X, Caberoy NB, Guo F, Shen C, Ji Y, Tian H, Wang H, Chen R, et al. (2017) Secretogranin III as a disease-associated ligand for antiangiogenic therapy of diabetic retinopathy. J Exp Med 214, 1029–1047. [PubMed: 28330905]

20. Rong X, Tian H, Yang L, Li W (2019) Function-first ligandomics for ocular vascular research and drug target discovery. Exp Eye Res 182, 57–64. [PubMed: 30904565]

21. Tang F, LeBlanc ME, Wang W, Liang D, Chen P, Chou T-H, Tian H, Li W (2019) Anti-secretogranin III therapy of oxygen-induced retinopathy with optimal safety. Angiogenesis 22, 369–382. [PubMed: 30644010]
22. Caberoy NB, Zhou Y, Jiang X, Alvarado G, Li W (2010) Efficient identification of tubby-binding proteins by an improved system of T7 phage display. J Mol Recognit 23, 74–83. [PubMed: 19718693]
23. Kingsley DM, Rinchik EM, Russell LB, Ottiger HP, Sutcliffe JG, Copeland NG, Jenkins NA (1990) Genetic ablation of a mouse gene expressed specifically in brain. EMBO J 9, 395–399 [PubMed: 2303033]
24. O'Neill JR (2019) An Overview of Mass Spectrometry-Based Methods for Functional Proteomics. Methods Mol Biol 1871, 179–196. [PubMed: 30276741]
25. Cabello-Aguilar S, Alame M, Kon-Sun-Tack F, Fau C, Lacroix M, Colinge J (2020) SingleCellSignalR: inference of intercellular networks from single-cell transcriptomics. Nucleic Acids Res 48, e55. [PubMed: 32196115]
26. Li W, Pang I-H, Pacheco MTF, Tian H (2018) Ligandomics: a paradigm shift in biological drug discovery. Drug Discov Today 23, 636–643. [PubMed: 29326083]
27. LeBlanc ME, Wang W, Ji Y, Tian H, Liu D, Zhang X, Li W (2019) Secretogranin III as a novel target for the therapy of choroidal neovascularization. Exp Eye Res 181, 120–126. [PubMed: 30633921]
28. Dai C, Wadge P, Ji L, Huang C, He Y, Tian H, Zuniga-Sanchez E, Bhatt A, Pang I-H, Su G et al. (2022) Secretogranin III stringently regulates pathological but not physiological angiogenesis in oxygen-induced retinopathy. Cell Mol Life Sci (In press)
29. Dai C, Webster KA, Bhatt A, Tian H, Su G, Li W (2021) Concurrent Physiological and Pathological Angiogenesis in Retinopathy of Prematurity and Emerging Therapies. Int J Mol Sci 22, 4809. [PubMed: 34062733]
30. Egawa G, Nakamizo S, Natsuaki Y, Doi H, Miyachi M, Kabashima K (2013) Intravital analysis of vascular permeability in mice using two-photon microscopy. Sci Rep 3, 1932. [PubMed: 23732999]
31. Cooper ME, Vranes D, Youssef S, Stacker SA, Cox AJ, Rizkalla B, Casley DJ, Bach LA, Kelly DJ, Gilbert RE (1999) Increased renal expression of vascular endothelial growth factor (VEGF) and its receptor VEGFR-2 in experimental diabetes. Diabetes 48, 2229–2239. [PubMed: 10535459]
32. Pino RM, Essner E (1981) Permeability of rat choriocapillaris to hemeproteins. Restriction of tracers by a fenestrated endothelium. J Histochem Cytochem 29, 281–290. [PubMed: 7252121]
33. Pino RM, Thouron CL (1983) Vascular permeability in the rat eye to endogenous albumin and immunoglobulin G (IgG) examined by immunohistochemical methods. J Histochem Cytochem 31, 411–416. [PubMed: 6827079]
34. Li W, Webster KA, LeBlanc ME, Tian H (2018) Secretogranin III: a diabetic retinopathy-selective angiogenic factor. Cell Mol Life Sci 75, 635–647. [PubMed: 28856381]
35. Holmes DIR, Zachary I (2005) The vascular endothelial growth factor (VEGF) family: angiogenic factors in health and disease. Genome Biol 6, 209. [PubMed: 15693956]
36. Maeda Y, Kudo S, Tsushima K, Sato E, Kubota C, Kayamori A, Bochimoto H, Koga D, Torii S, Gomi H, et al. (2018) Impaired Processing of Prohormones in Secretogranin III-Null Mice Causes Maladaptation to an Inadequate Diet and Stress. Endocrinology 159, 1213–1227. [PubMed: 29281094]
37. Tanabe A, Yanagiya T, Iida A, Saito S, Sekine A, Takahashi A, Nakamura T, Tsunoda T, Kamohara S, Nakata Y, et al. (2007) Functional single-nucleotide polymorphisms in the secretogranin III (SCG3) gene that form secretory granules with appetite-related neuropeptides are associated with obesity. J Clin Endocrinol Metab 92, 1145–1154. [PubMed: 17200173]
38. Kirchmair R, Egger M, Walter DH, Eisterer W, Niederwanger A, Woell E, Nagl M, Pedrini M, Murayama T, Frauscher S, et al. (2004) Secretoneurin, an angiogenic neuropeptide, induces postnatal vasculogenesis. Circulation 110, 1121–1127. [PubMed: 15326074]
39. Hannon PR, Duffy DM, Rosewell KL, Brannstrom M, Akin JW, Curry TE Jr (2018) Ovulatory Induction of SCG2 in Human, Nonhuman Primate, and Rodent Granulosa Cells Stimulates Ovarian Angiogenesis. Endocrinology 159, 2447–2458. [PubMed: 29648638]

40. Fang C, Dai L, Wang C, Fan C, Yu Y, Yang L, Deng H, Zhou Z (2021) Secretogranin II impairs tumor growth and angiogenesis by promoting degradation of hypoxia-inducible factor-1α in colorectal cancer. Mol Oncol 15, 3513–3526. [PubMed: 34160138]
41. Helle KB, Corti A (2015) Chromogranin A: a paradoxical player in angiogenesis and vascular biology. Cell Mol Life Sci 72, 339–348. [PubMed: 25297920]
42. Crippa L, Bianco M, Colombo B, Gasparri AM, Ferrero E, Loh YP, Curnis F, Corti A (2013) A new chromogranin A-dependent angiogenic switch activated by thrombin. Blood 121, 392–402. [PubMed: 23190532]
43. Moss AC, Jacobson GM, Walker LE, Blake NW, Marshall E, Coulson JM (2009) SCG3 transcript in peripheral blood is a prognostic biomarker for REST-deficient small cell lung cancer. Clin Cancer Res 15, 274–283. [PubMed: 19118055]
44. Portela-Gomes GM, Grimelius L, Stridsberg M (2010) Secretogranin III in human neuroendocrine tumours: a comparative immunohistochemical study with chromogranins A and B and secretogranin II. Regul Pept 165, 30–35. [PubMed: 20550951]
45. Wang Y, Ji N, Wang J, Cao J, Li D, Zhang Y, Zhang L (2021) SCG3 Protein Expression in Glioma Associates With less Malignancy and Favorable Clinical Outcomes. Pathol Oncol Res 27, 594931. [PubMed: 34257545]
46. Yang Y, Zhang Y, Cao Z, Ji H, Yang X, Iwamoto H, Wahlberg E, Lanne T, Sun B, Cao Y (2013) Anti-VEGF- and anti-VEGF receptor-induced vascular alteration in mouse healthy tissues. Proc Natl Acad Sci U S A 110, 12018–12023. [PubMed: 23818623]
47. Calvo PM, Pastor AM, de la Cruz RR (2018) Vascular endothelial growth factor: an essential neurotrophic factor for motoneurons? Neural Regen Res 13, 1181–1182. [PubMed: 30028320]
48. Byeon SH, Lee SC, Choi SH, Lee H-K, Lee JH, Chu YK, Kwon OW (2010) Vascular endothelial growth factor as an autocrine survival factor for retinal pigment epithelial cells under oxidative stress via the VEGF-R2/PI3K/Akt. Invest Ophthalmol Vis Sci 51, 1190–1197. [PubMed: 19834034]
49. Sepah YJ, Sadiq MA, Boyer D, Callanan D, Gallemore R, Bennett M, Marcus D, Halperin L, Hassan M, Campochiaro PA, et al. (2016) Twenty-four-Month Outcomes of the Ranibizumab for Edema of the Macula in Diabetes - Protocol 3 with High Dose (READ-3) Study. Ophthalmology 123, 2581–2587. [PubMed: 27707550]
50. Ho AC, Busbee BG, Regillo CD, Wieland MR, Van Everen SA, Li Z, Rubio RG, Lai P, HARBOR Study Group (2014) Twenty-four-month efficacy and safety of 0.5 mg or 2.0 mg ranibizumab in patients with subfoveal neovascular age-related macular degeneration. Ophthalmology 121, 2181–2192. [PubMed: 25015215]
51. LeBlanc ME, Wang W, Caberoy NB, Chen X, Guo F, Alvarado G, Shen C, Wang F, Wang H, Chen R, et al. (2015) Hepatoma-derived growth factor-related protein-3 is a novel angiogenic factor. PLoS One 10, e0127904. [PubMed: 25996149]
52. Wang W, LeBlanc ME, Chen X, Chen P, Ji Y, Brewer M, Tian H, Spring SR, Webster KA, Li W (2017) Pathogenic role and therapeutic potential of pleiotrophin in mouse models of ocular vascular disease. Angiogenesis 20, 479–492. [PubMed: 28447229]
53. Tokuda K, Baron B, Kuramitsu Y, Kitagawa T, Tokuda N, Morishige N, Kobayashi M, Kimura K, Nakamura K, Sonoda K-H (2018) Optimization of fixative solution for retinal morphology: a comparison with Davidson's fixative and other fixation solutions. Jpn J Ophthalmol 62, 481–490. [PubMed: 29691783]

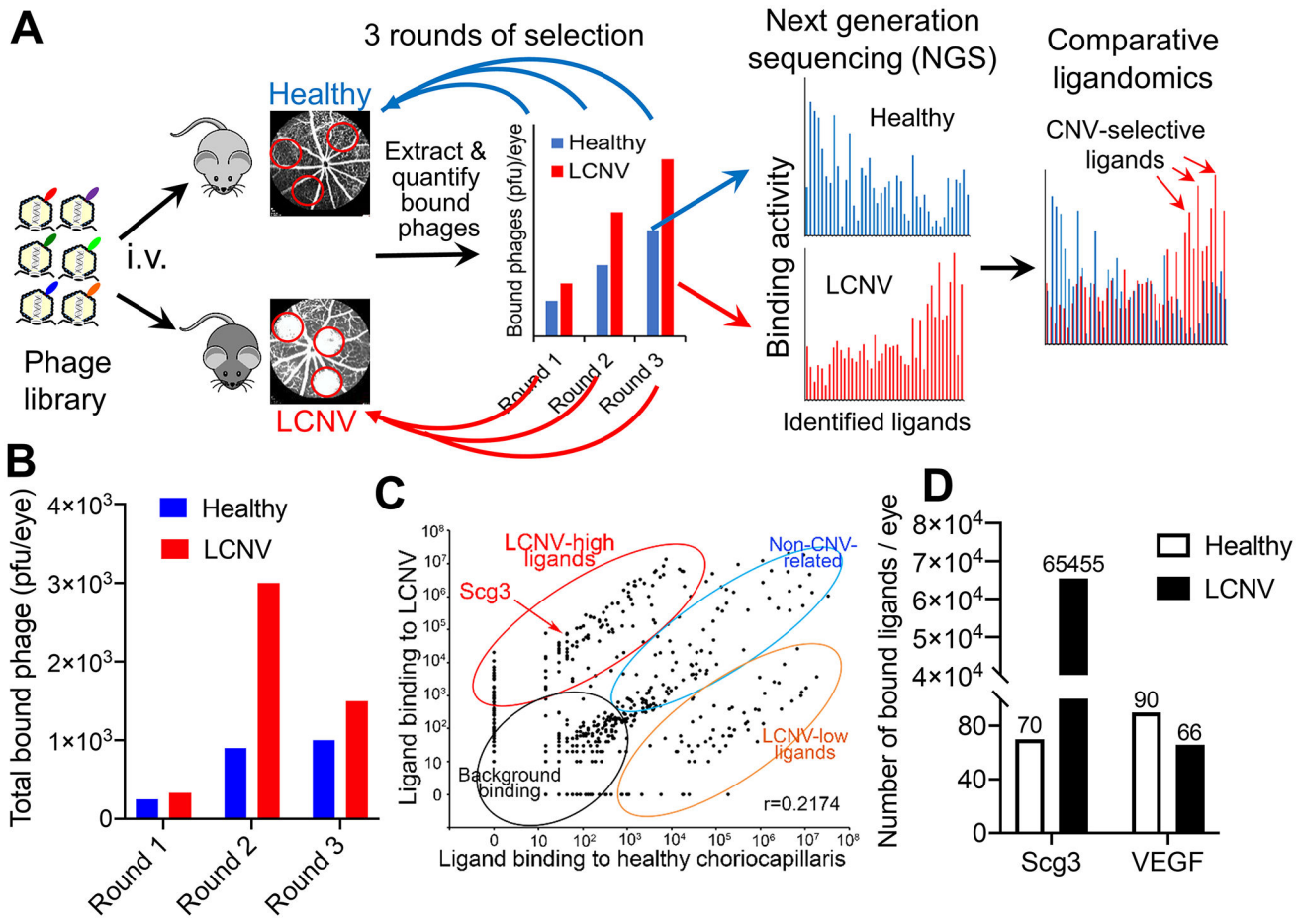

Fig. 1.

Comparative ligandomics profiling of LCNV vs. healthy choroids to identify Scg3 as a disease-selective endothelial ligand. (A) Schematic of comparative ligandomics. Open reading frame phage display (OPD) cDNA libraries were purified and injected i.v. into anesthetized mice with or without LCNV for 3 rounds of *in vivo* binding selection to choroidal vessels. Enriched vessel-bound clones were identified by NGS and quantitatively compared. (B) Quantification of vessel-bound phage clones at Round 1 (1 min washing), 2 (3 min washing) and 3 (7 min washing) with increased washing time for binding stringency. (C) Binding activity plot of all enriched vessel-binding ligands. Pearson correlation coefficient (r) for all ligands binding to LCNV versus healthy choriocapillaris is 0.2174. (D) Comparative ligandomics identifies Scg3, but not VEGF, as a LCNV-selective endothelial ligand.

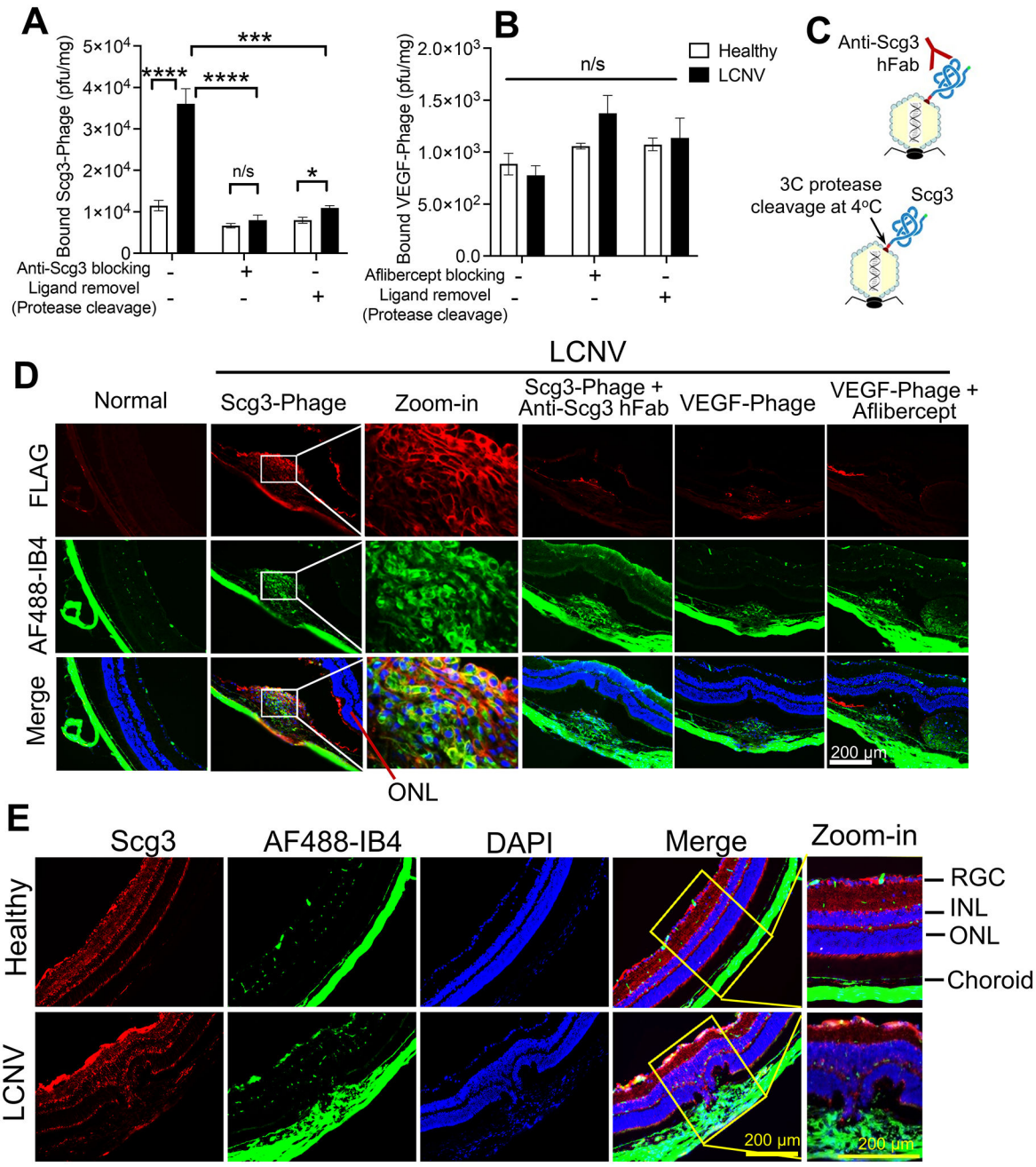

Fig. 2.

Independent verification of Scg3, but not VEGF, as a LCNV-selective endothelial ligand. (A,B) *In vivo* ligand binding assay to quantify Scg3-Phage and VEGF-Phage binding to healthy and LCNV choroidal vessels. (A) Clonal Scg3-Phage binding to LCNV was blocked by preincubation with anti-Scg3 hFab (4 μg/ml) or HRV 3C protease (100 units/ml) to cleave displayed Scg3 from the phage surface (see C). Vessel-bound Scg3-Phage was quantified by plaque assay. n=10 eyes in 5 mice/group (Scg3-Phage) and 6 eyes in 3 mice/group (Scg3-Phage with anti-Scg3 hFab blocking or 3C protease treatment). (B) Clonal VEGF-Phage binding as described in A. Aflibercept (4 μg/ml) or HRV 3C was used to block VEGF

binding. n=6 eyes in 3 mice/group. ±SEM; *P<0.05, ***P<0.001, ****P<0.0001, n/s for not significant; One-way ANOVA test. (C) Illustration of Scg3 blockade by anti-Scg3 hFab (top) or Scg3 ligand removal from the T7 phage surface by HRV 3C protease cleavage (bottom) in A and B. (D) Functional immunohistochemistry to visualize Scg3-Phage binding to LCNV but not healthy choroidal vessels. FLAG-tagged Scg3-Phage or VEGF-Phage was preincubated with or without anti-Scg3 hFab or aflibercept, respectively, for *in vivo* binding as described in A and B. After perfusion and *in situ* fixation, retinal sections were incubated with anti-FLAG mAb (red) and AF488-IB4 (green, staining vessels) to visualize vessel-bound Scg3-Phage. (E) Immunohistochemistry to detect Scg3 expression (red) in healthy and LCNV eyes. Vessels were stained with anti-CD31 mAb (green). Scale bar = 200 μm.

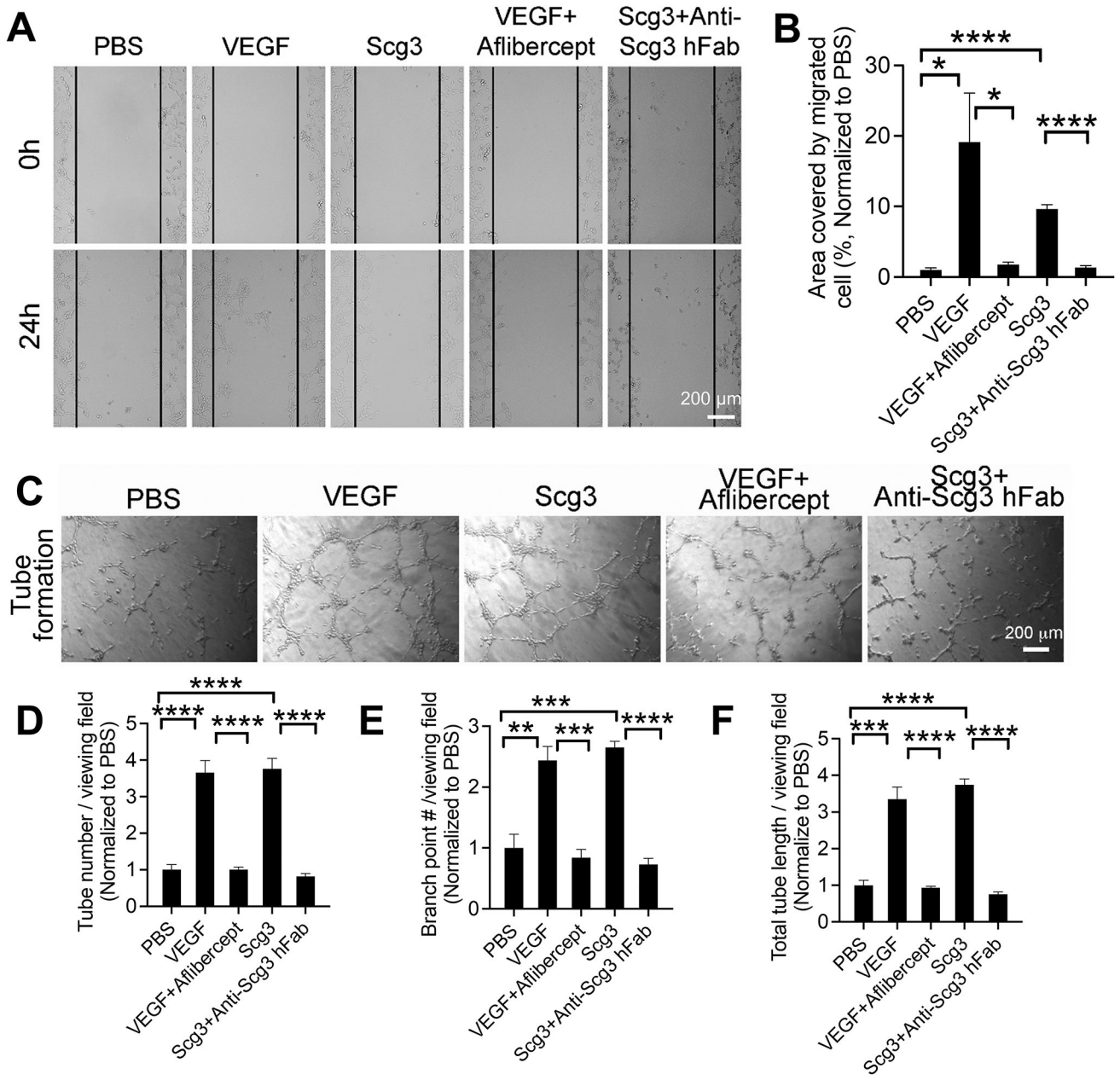

Fig. 3.

Neutralizing activity of anti-Scg3 hFab. (A) Representative image of wound healing migration assay using HUVECs. (B) Quantification of migrated cells in A. n=6 wells/group. (C) Tube formation assay. (D) Quantification of tube number in C. (E) Quantification of tube length in C. (F) Quantification of branch points in C. n=5 wells/group for D-F. Scale bar = 200 μm. ±SEM; **P*<0.05, ***P*<0.01, ****P*<0.001, *****P*<0.0001; one-way ANOVA test.

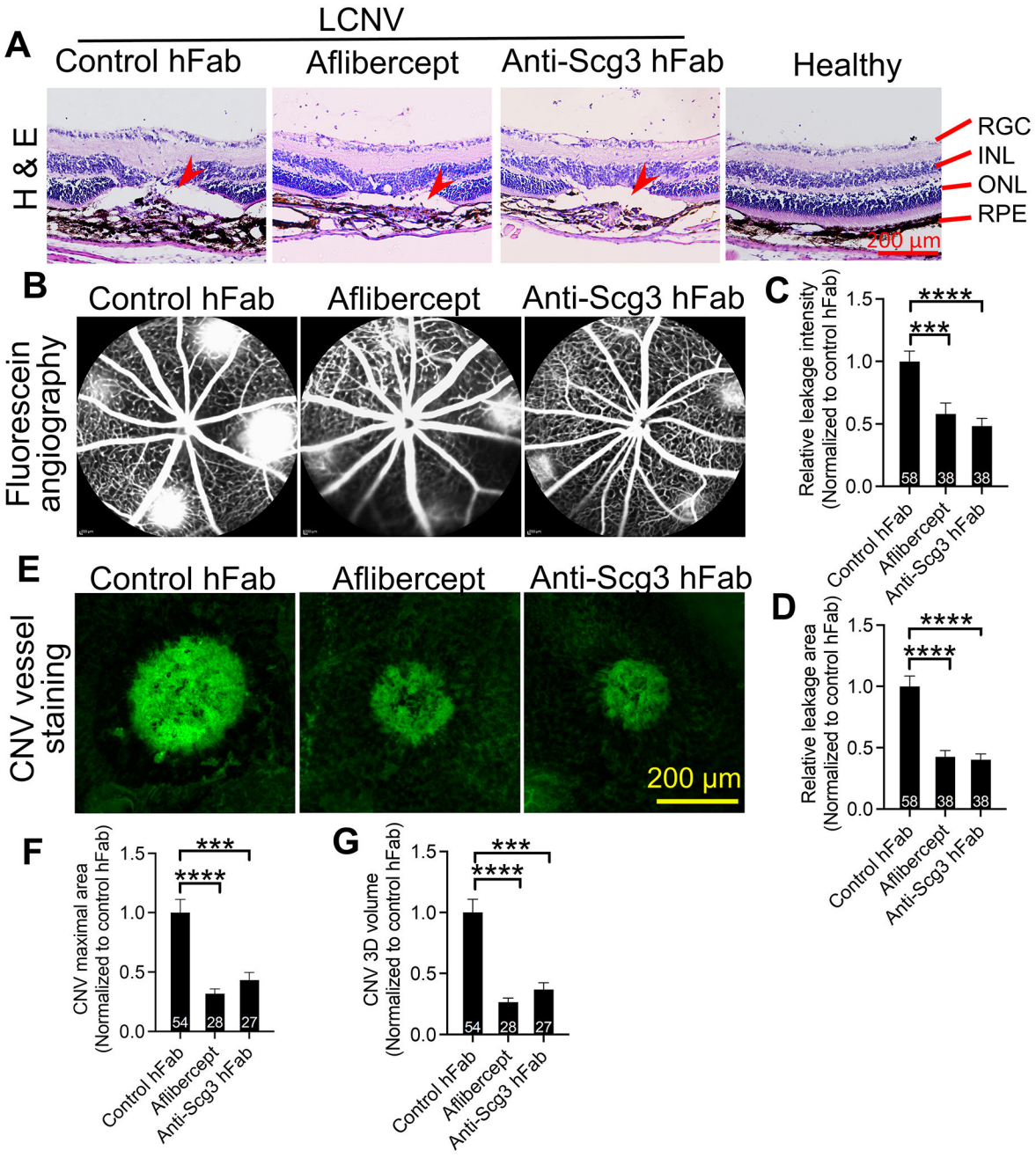

Fig. 4.

Anti-Scg3 hFab alleviates LCNV. (A) H&E staining of LCNV after treatment with anti-Scg3 hFab, aflibercept or control hFab (2 µg/1 µl/eye). Mice were induced for LCNV on Day 0, received intravitreal treatment on Day 3 and isolated for H&E staining on Day 7. (B) Representative images of fluorescein angiography (FA) for LCNV in mice on Day 7. Treatment is described in A. (C) Quantitation of CNV leakage intensity in B. (D) Quantification of CNV leakage area in B. (E) Representative images of LCNV in flat-mounted RPE eyecups stained with AF488-IB4. RPE eyecups were isolated from B. Scale bar = 200 µm. (F) Quantitation of CNV maximal area in E. (G) Quantification of CNV

3D volume in E. n (# laser spots/group) is indicated inside graphs. ±SEM; ***P<0.001, ****P<0.0001; one-way ANOVA test.

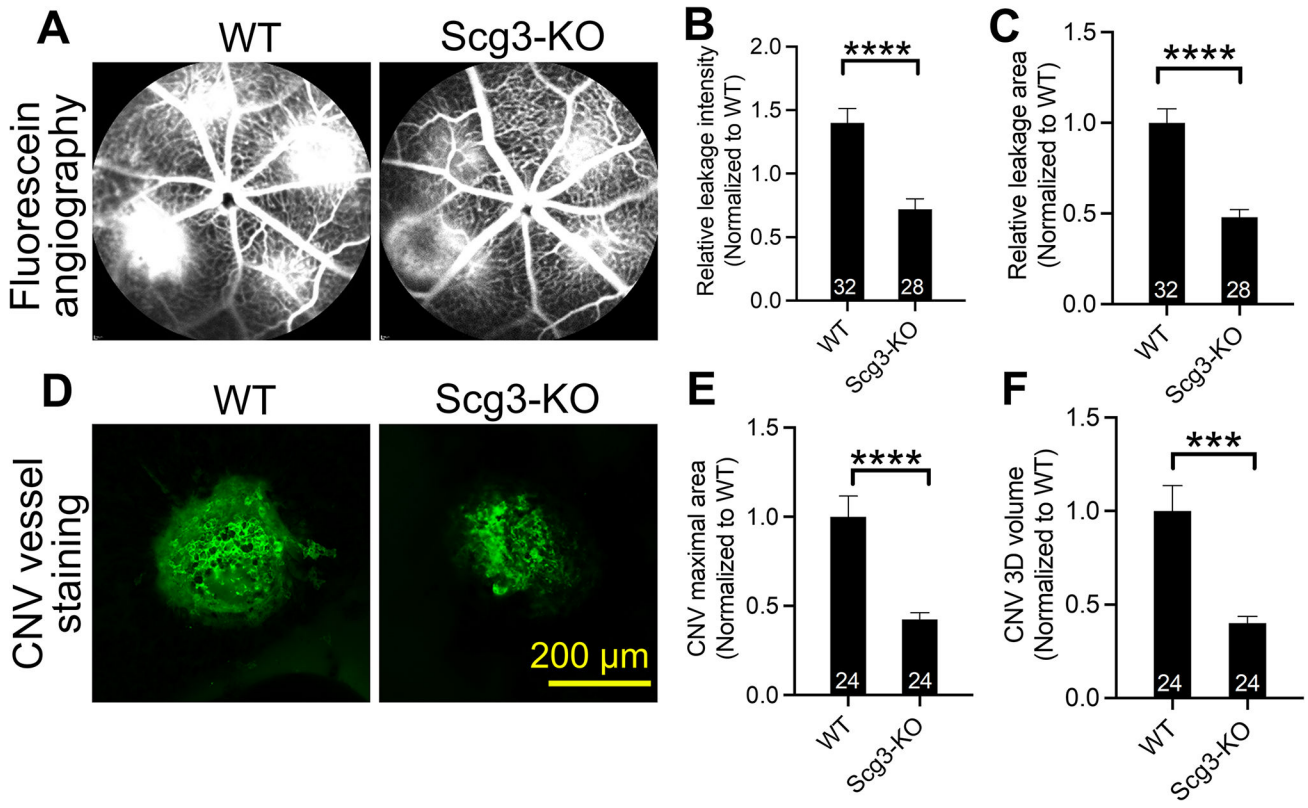

Fig. 5.

LCNV severity in Scg3-KO mice. (A) Representative images of FA for LCVN in $Scg3^{+/+}$ and $Scg3^{-/-}$ mice at 7 days post laser photocoagulation. (B) Quantification of CNV leakage intensity in A. (C) Quantification of CNV leakage area in A. (D) Representative images of LCNV in flat-mount RPE eyecups stained with AF488-IB4. RPE eyecups were isolated from A. Scale bar = 200 μm. (E) Quantification of CNV maximal area in D. (F) Quantification of CNV 3D volume in D. n (# laser spots/group) is indicated inside graphs. ±SEM; ***P<0.001, ****P<0.0001; one-way ANOVA test.

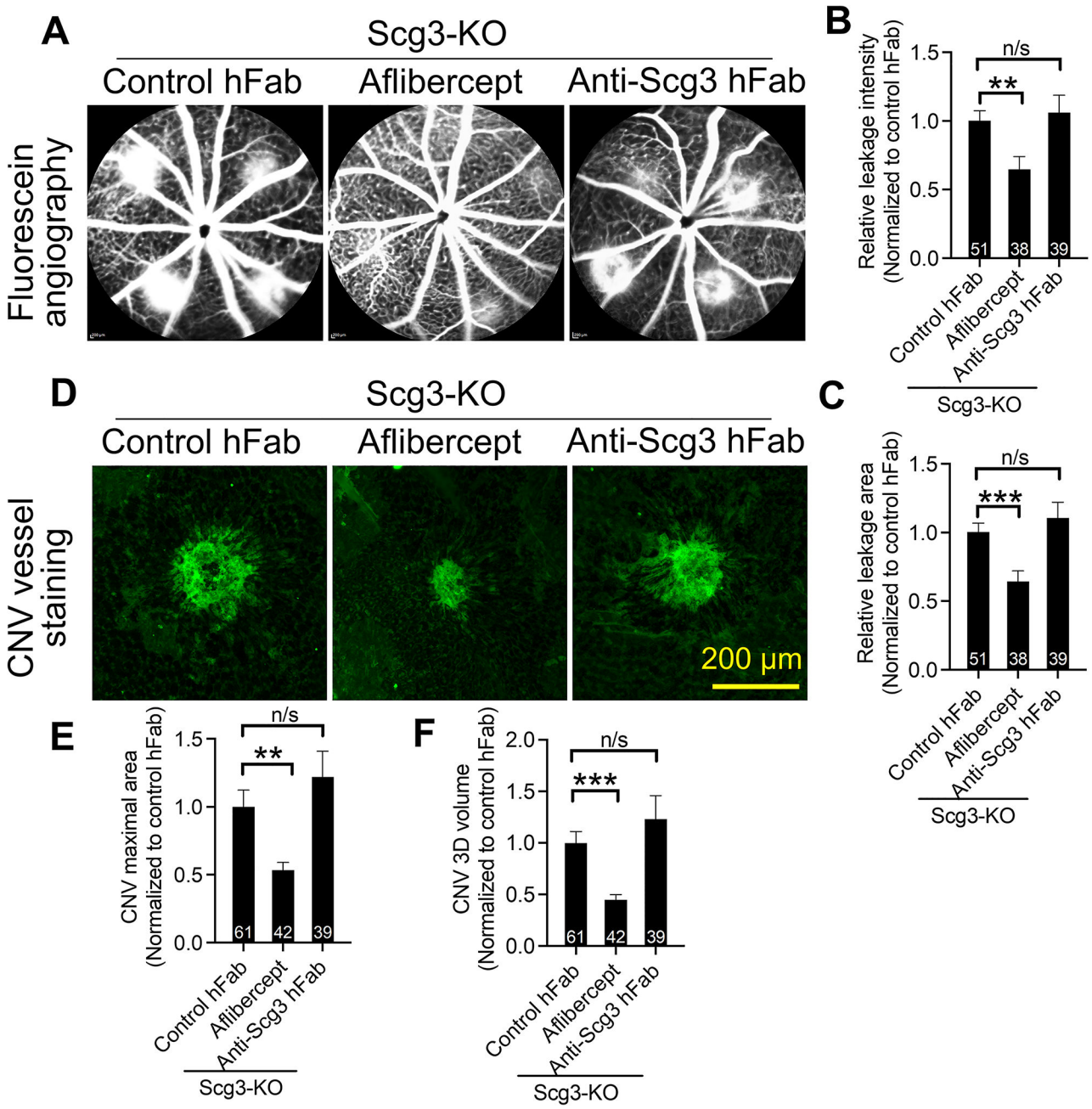

Fig. 6.

Anti-angiogenic therapy in Scg3-null mice. Scg3$^{-/-}$ mice were treated with laser on Day 0 to induce CNV and intravitreally treated with anti-Scg3 hFab, aflibercept or control hFab (2 μg/1 μl/eye) at 3 days post laser photocoagulation, as described in Fig. 4. (A) Representative images of FA at Day 7. (B) Quantification of CNV leakage intensity in A. (C) Quantification of CNV leakage area in A. (D) Representative images of CNV in flat-mount RPE eyecups stained with AF488-IB4. RPE eyecups were isolated from A. Scale bar = 200 μm. (E) Quantification of CNV maximal area in D. (F) Quantification of CNV 3D volume in D.

n (# laser spots/group) is indicated inside graphs. ±SEM; ** P<0.01, *** P<0.001; n/s, not significant; one-way ANOVA test.